Supporting Material

Mechanical Stability and Reversible Fracture of Vault Particles

Aida Llauró,[†] Pablo Guerra,[‡] Nerea Irigoyen,[§] José F. Rodríguez,[¶] Núria Verdaguer,[‡] Pedro J. de Pablo,[†,*]

[†]Departamento de Física de la Materia Condensada, UAM, Francisco Tomás y Valiente 7,28049-Madrid, Spain.

[‡]Institut de Biologia Molecular de Barcelona, CSIC. Baldiri i Reixac 10, 08028-Barcelona, Spain.

[§]Division of Virology, Department of Pathology, University of Cambridge, Tennis Court, Cambridge CB2 1QP, United Kingdom.

[¶]Centro Nacional de Biotecnología, CSIC, Calle Darwin nº 3, 28049-Madrid, Spain.

*****Correspondence: p.j.depablo@uam.es

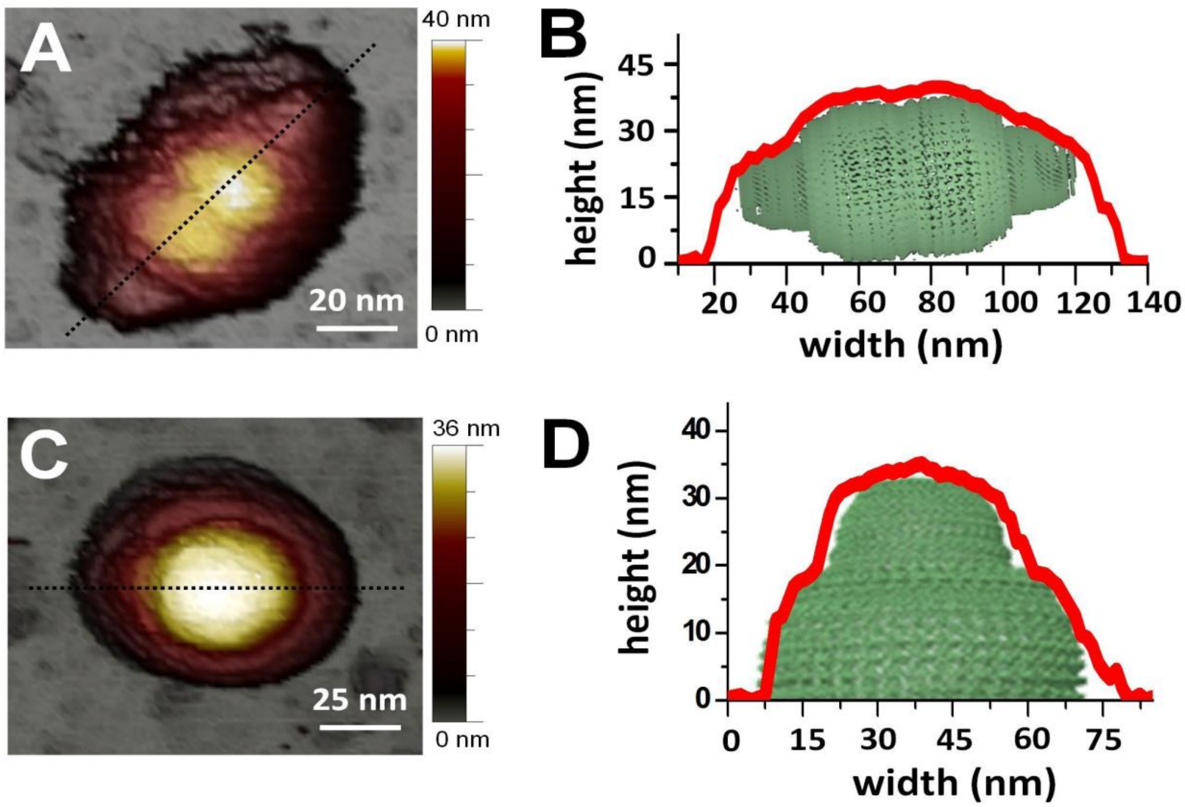

FIGURE S1. High-resolution AFM topographies of an entire reclining particle and a half-vault. (*A*) Topographical image of a reclining particle. (B) Longitudinal profile taken along the dotted black line in Fig. A. The height profile (*red line*) shows an excellent agreement with the X-Ray data of the vault structure. In this case, the vault is tilted about 5 degrees from the substrate. (*C*) AFM topography of a half vault with the cap facing up. (D) Profile taken along the dotted black line in Fig. C. Again, the dimensions agree with those obtained by X-Ray and EM.[3]

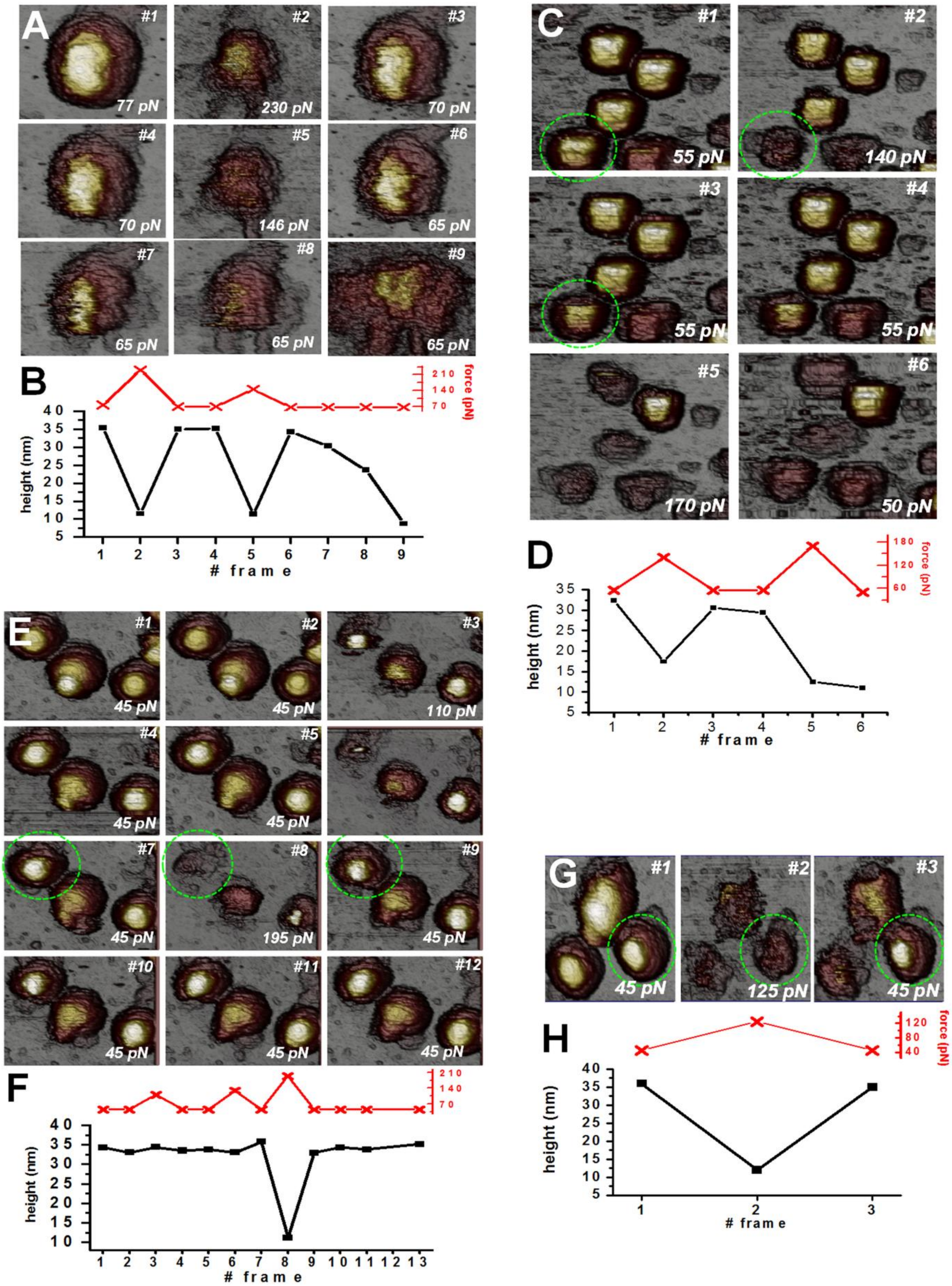

FIGURE S2. Half-vault deformation depending on force imaging. (*A*) Topographical images are time ordered and labeled with its corresponding imaging force. (*B*) (*top*) Imaging force evolution of Fig. S2 *A*. (*bottom*) Maximal height evolution of Fig. S2 *A*. (*C*-*D*), (*E*-*F*), and (*G*-*H*) correspond, respectively, to three more cases. The height evolution for these cases accounts for the half-vault circled with a green dotted line.

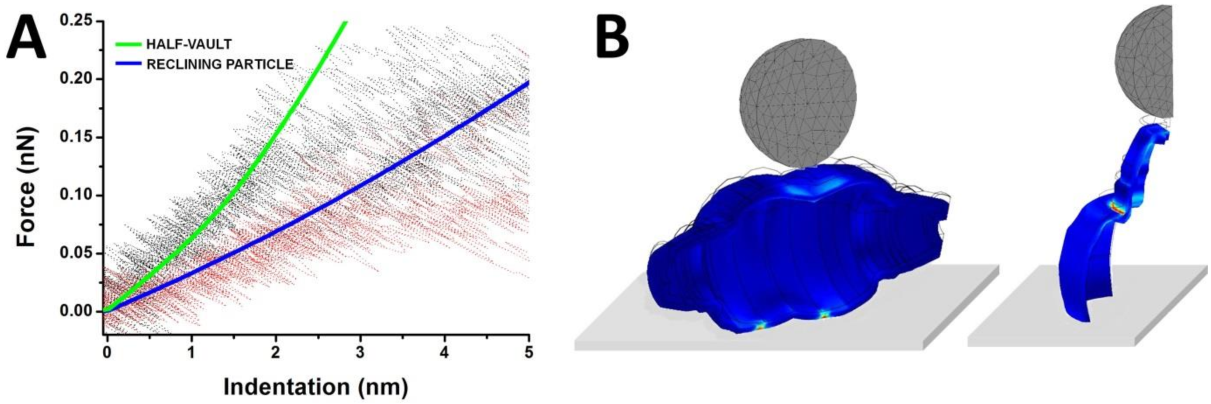

FIGURE S3. Finite Element Analysis. (*A*) FIC obtained in the Finite Element simulation for a half-vault (*green*) and a reclining particle (*blue*) when Young's modulus was set to E=700 MPa. On the background we have overlaid the experimental curves for 26 different half-vaults (black) and 13 different reclining particles (red). (*B*) (*left*) Image of a half segment of a reclining particle with a 6 nm indentation; again, the colors indicate the von Misses stress distribution. (*right*) Image of a quarter segment of a half-vault with a 6 nm indentation, the colors indicating the distribution of the von Misses stress.

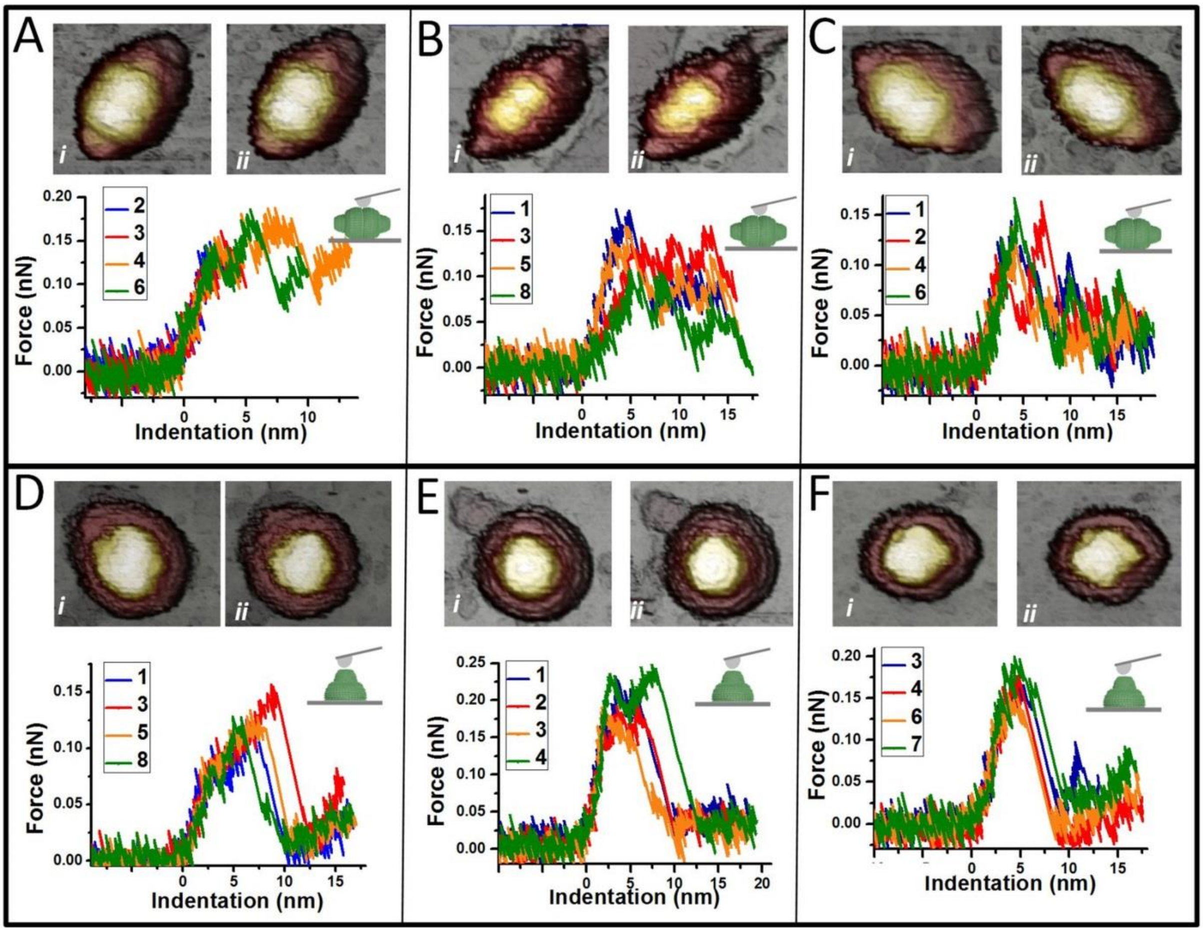

FIGURE S4. Cyclic loading. (*A*) Some of the FIC performed on top of the reclining particle shown in *i*. The numbers in the legend indicate the order of the curves. The image of the particle after the cyclic loading is represented in *ii*. (*B, C*) Two more examples, as in A. (*D, E, F*) Cycle loading experiments performed on half-vaults.

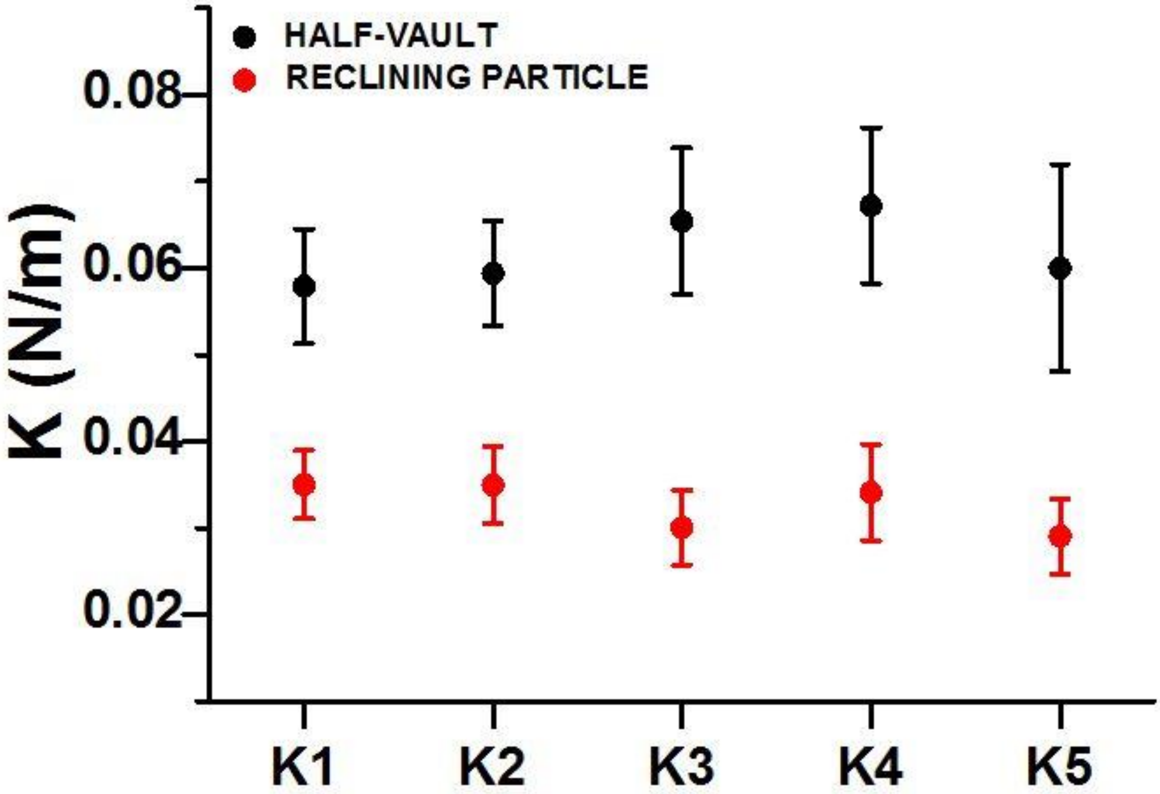

FIGURE S5. Evolution of the spring constant. The grah shows the evolution of the average spring costant value during the first indentation cycle (corresponding to 5 consecutive FICs). The values were obtained from 21 half-vaults and 13 reclinging particles, respectively. Each FIC was perfomed beyond the breaking limit.

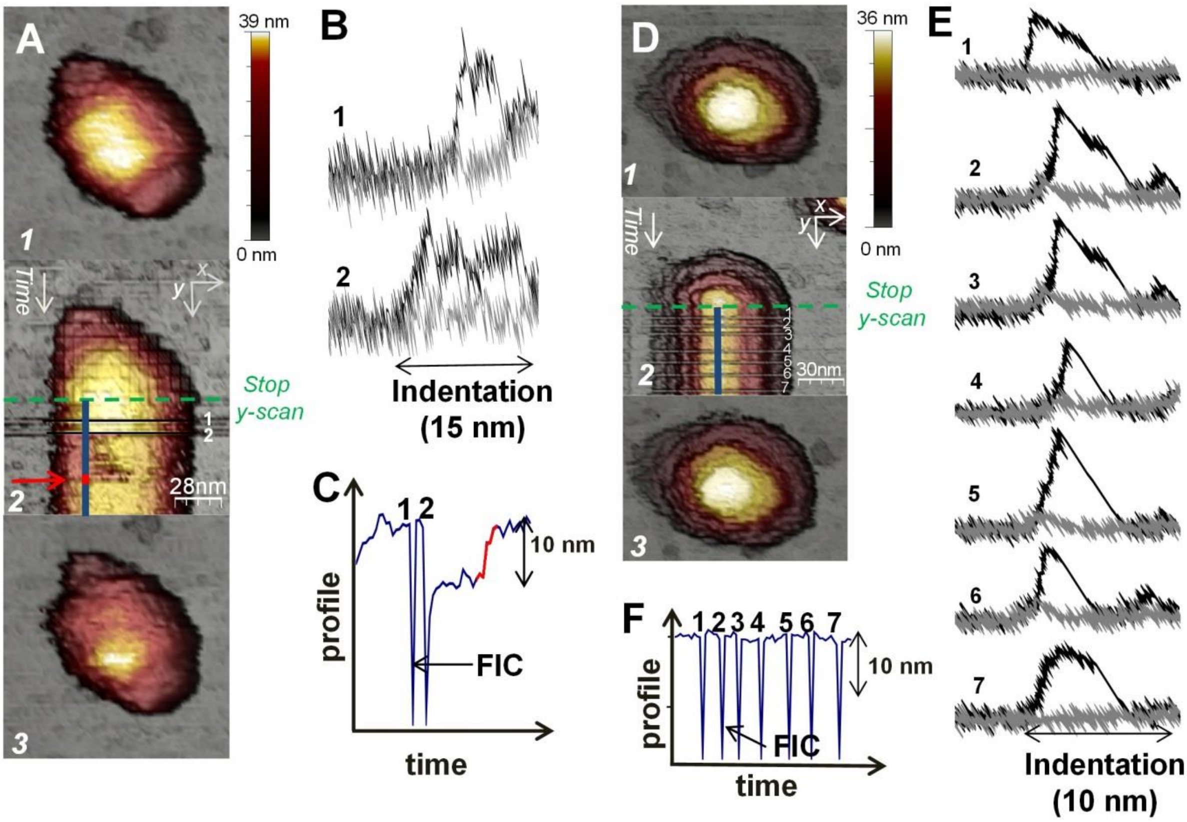

FIGURE S6. Monitoring of the topography in a stopped y-scan (*A*) Image of a reclining particle: (1) before the indentations, (2) during the indentations, and (3) after the indentations. All images were taken from top to bottom. In figure A *2*, the dashed green line indicates the place where the tip stopped scanning in the y-direction. Therefore, from this line, the tip was placed on top of the structure and FICs started. Each black line in figure A *2* corresponds to a different FIC. After the second indentation, the structure of the particle was damaged, as a partial loss in height was observed (darker zone on top of the structure). Further imaging of this profile showed a recovery of the structure (*red arrow*). (*B*) The indentations performed on the top of the structure, the number of each curve corresponding to the order in which they were performed. (*C*) Topographic profile corresponding to the solid blue line depicted in figure A *2*. In this profile, each FIC is represented as a sharp decrease. After the second FIC, the structure lost 10 nm in height that was later recovered (*red line*). (*D, E, F*) The same experiment performed on a half-vault. In this case, the particle does not display any topographical changes. However, some backward curves present a recovery (2, 3, 4, 5, and 6) whereas others do not (1 and 7). These latter cases correspond to recoveries occurring during the non-contact part of the curve (flattened region), which we classified as medium recovery times (650ms<RT<2s).

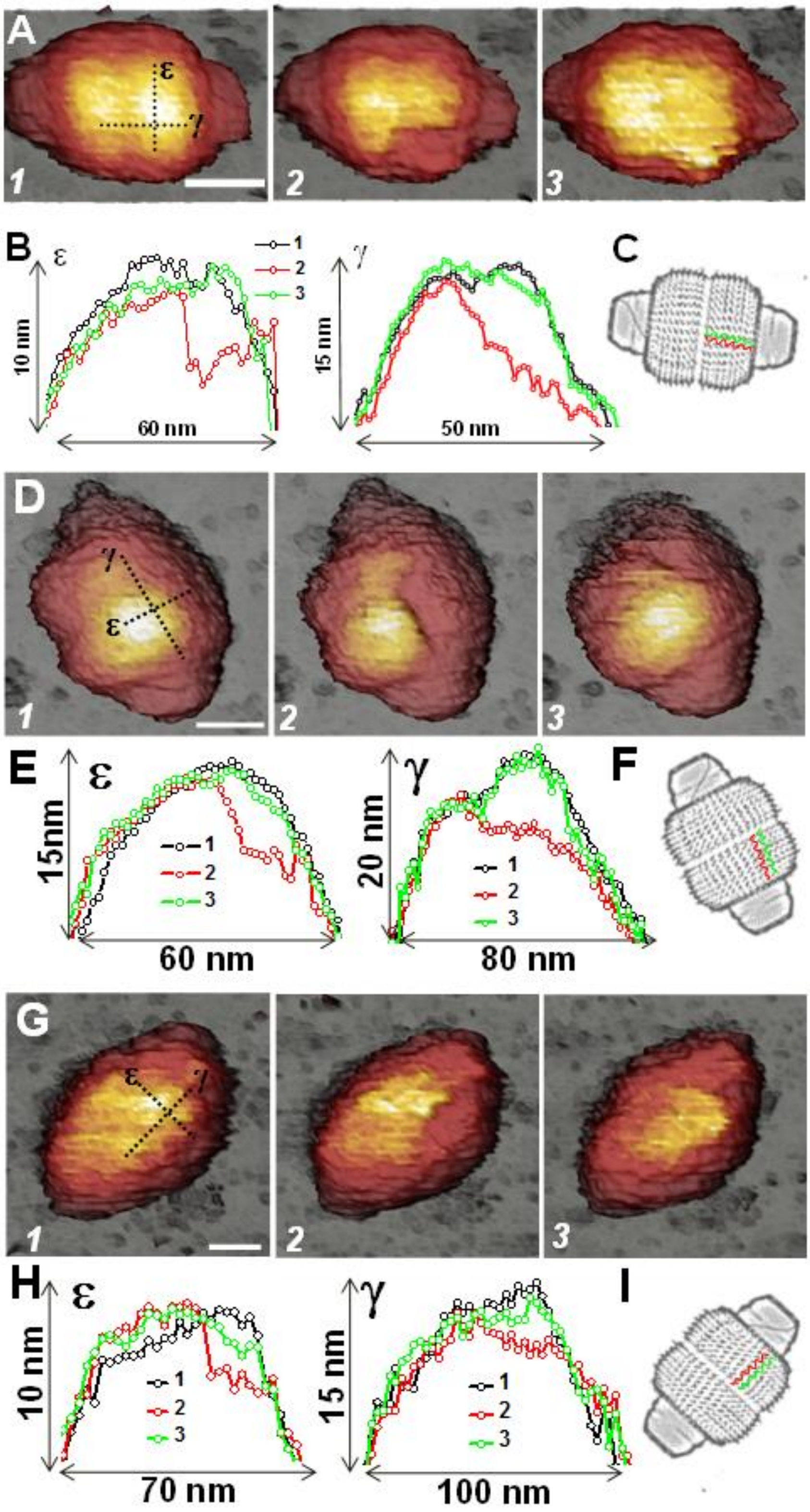

FIGURE S7. Reversible failure of vaults (*A*) Consecutive images of a reclining particle: (1) before the fracture, (2) just after the fracture, and (3) after the recovery. (*B*) Profiles ε and γ depicted with dotted black lines in Figure A1: before the fracture (*black*), after the fracture (*red*), and after the recovery (*green*). (*C*) Picture showing the line of fracture aligned between two neighboring MVPs (in *red*), with the depressed region highlighted in pink. (*D, E, F*) and (*G, H, I*) correspond, respectively, to two more cases of slow reversible fracture.

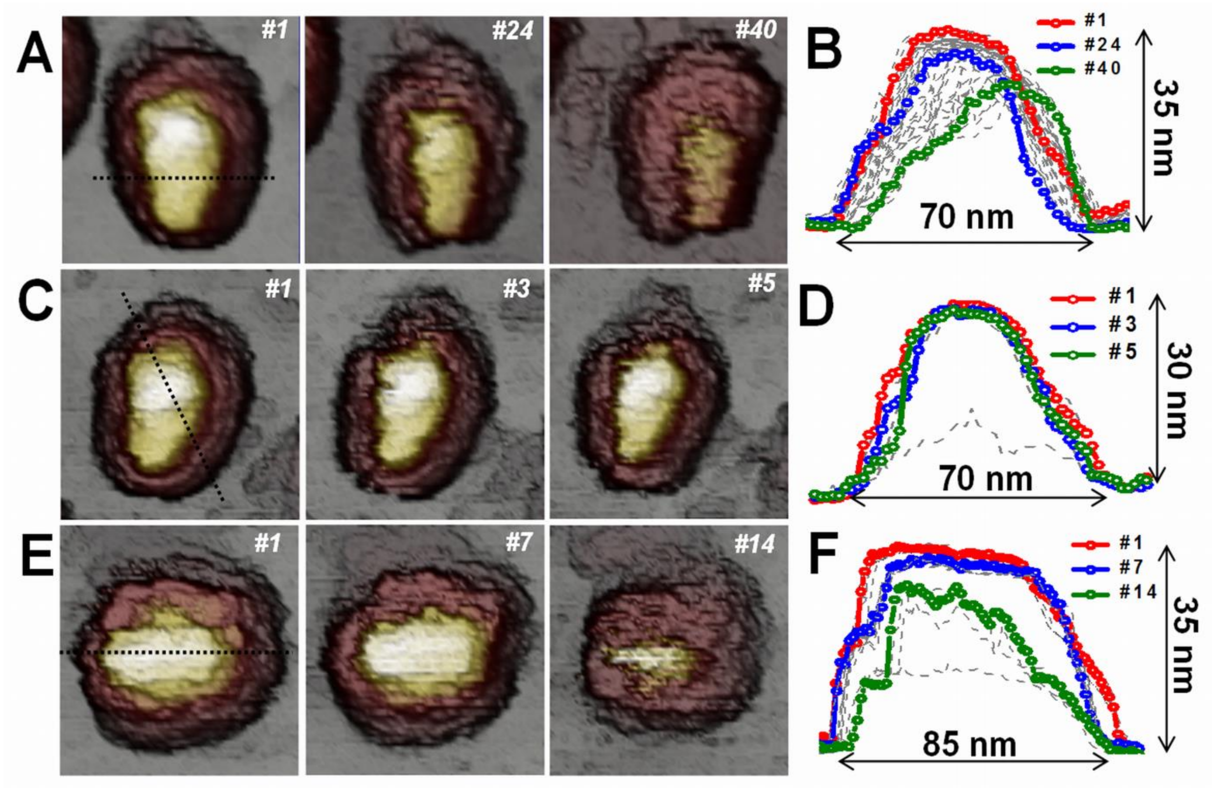

FIGURE S8. Three cases of fatigue experiments on half-vaults (*A*) Evolution of the topographical images of a half-vault imaged at 70 pN. Images are time ordered and labeled with the number of its corresponding frame. In this case, the particle was imaged 40 times, which corresponds to a time of 90 minutes. (*B*) Evolution of the profile taken along the dotted black line of Figure A-1. The profiles corresponding to frames 1, 24, and 40 are depicted in red, blue, and green, respectively. The rest of the profiles are depicted in grey. (*C*, *D*) and (*E*,*F*) correspond, respectively, to two more cases. The imaging force for these cases was about 75 pN.

Movie 1. Mechanical fatigue of a half-vault. This movie indicates the temporal evolution of figure 6.